NJC

PAPER

View Article Online
View Journal | View Issue

Cite this: *New J. Chem.*, 2018, **42**, 19144

Structural and morphological aspects of (fluoro)quinolone delivery by layered double hydroxide nanoparticles†

Yadira Salguero,[a] Mónica Cristina García,[b] Giuliana Mosconi[c] and Ricardo Rojas *[a]

Layered double hydroxides (LDHs) have been proposed as delivery systems (DSs) of (fluoro)quinolones (QLNs) to overcome their low bioavailability and to prevent the emergence of resistant bacteria. Both LDH-DS synthesis as nanoparticles (NPs) and QLN interactions with the metal ions that constitute the layers are essential to improve their physicochemical, biopharmaceutical and antimicrobial properties. Here, LDH-DSs containing the basic form of nalidixic acid (Nal), used as a probe, were obtained by coprecipitation at variable and constant pH (LDH-Nal-pHvar and LDH-Nal-pHcte, respectively). For both syntheses, LDH NPs containing Nal anions (LDH-Nal-NPs), with sizes between 30 and 40 nm, were obtained. A coordination compound ($Mg(Nal)_2{\cdot}4H_2O$, $Mg(Nal)_2$) was also concurrent for LDH-Nal-pHcte, which modulated the drug release profile and antimicrobial properties of the LDH-Nal-NPs. Thus, Nal release from LDH-Nal-pHvar was produced mainly by anion exchange. The best fits, obtained for the Higuchi model, showed rate constants dependent on the exchanging anions (k_H = 0.88 and 1.53 for NaCl 0.9% and buffer phosphate 0.05 M, pH = 7.4, respectively). The nanometric size of LDH-Nal-pHvar as well as its faster release rate allowed a minimum inhibitory concentration decrease (MIC = 32 μg mL^{-1}) compared to the pure drug (MIC = 128 μg mL^{-1}). Instead, the presence of $Mg(Nal)_2$ in LDH-Nal-pHcte led to a more sustained and media independent Nal release, but a lower MIC (64 μg mL^{-1}) than LDH-Nal-pHvar.

Received 24th July 2018,
Accepted 31st October 2018

DOI: 10.1039/c8nj03072c

rsc.li/njc

1. Introduction

(Fluoro)quinolones (QLNs), due to their variety, broad-spectrum bactericidal activity and efficacy, are widely used for therapeutic and prophylactic purposes.[1] Delivery systems (DSs) are increasingly studied for QLNs to reduce their fluctuations in plasma concentration, to protect them from degradation and to increase their bioavailability.[2] Also, DSs are intended to produce antimicrobial levels above the minimal inhibitory concentration (MIC) for longer times, preventing the resistance developed below it.[3] Organic matrixes (polymeric particles, liposomes or dendrimers) are mainly studied as hosts for QLNs[2,4,5] but the inorganic ones (carbon nanotubes, iron oxides, clays and layered double hydroxides (LDHs)) are receiving increasing attention.[4,6,7]

LDHs are inorganic anion exchangers that have been studied as matrixes in DSs for anionic drugs, including anti-inflammatories,[8] anticancer agents[9] or antimicrobials.[10,11] Their structure can be described as a stack of brucite-like layers with a general formula $[M^{II}_{1-x}M^{III}_{x}(OH)_2]A_{n/x}{\cdot}mH_2O$ (where M^{II} = Mg^{2+}, Ca^{2+}, Zn^{2+}, ...; M^{III} = Al^{3+}, Fe^{3+}, ... and A^{n-} is the interlayer anion).[12] The anionic drugs are placed between the layers and released by either anion exchange or dissolution of the host layers.[13] Release profile modification[14] as well as increased drug solubility and stability[15,16] are among the described advantages of LDHs.

LDHs have been proposed as hosts of anionic QLNs such as the basic form of nalidixic acid (HNal), enrofloxacin, ciprofloxacin and norfloxacin.[17–22] The obtained DSs exhibited modified release kinetics, while the bacteriological studies performed indicated that the antimicrobial activity against both Gram-positive and Gram-negative bacteria was maintained.[18,23] It has also been proposed that LDH nanoparticles (LDH-NPs) establish electrostatic

[a] *INFIQC-CONICET, Departamento de Fisicoquímica, Facultad de Ciencias Químicas, Universidad Nacional de Córdoba. Ciudad Universitaria, X5000HUA, Córdoba, Argentina. E-mail: rrojas@fcq.unc.edu.ar, yadisalgueros@gmail.com*
[b] *UNITEFA-CONICET, Departamento de Ciencias Farmacéuticas. Facultad de Ciencias Químicas, Universidad Nacional de Córdoba. Ciudad Universitaria, X5000HUA, Córdoba, Argentina. E-mail: mgarcia@fcq.unc.edu.ar*
[c] *IPQA-CONICET, Departamento de Química Orgánica, Facultad de Ciencias Químicas, Universidad Nacional de Córdoba. Ciudad Universitaria, X5000HUA, Córdoba, Argentina. E-mail: mosconigiuliana@gmail.com*

† Electronic supplementary information (ESI) available: Analysis of the synthesis parameters by titrations of metal salt solutions in presence and absence of HNal. Study of Nal interaction with LDH layers by Nal sorption isotherm on LDH-Cl. Bacteria count of lawn cultures of MIC determinations. See DOI: 10.1039/c8nj03072c

interactions with the membrane of both types of bacteria.[24] This interaction leads to membrane disruption, bacterial aggregation and membrane charging reduction that would potentially synergize with the action of intercalated QLNs. Nevertheless, the synthesis of LDH-NPs containing QLNs has not yet been described to our knowledge.

Another unexplored feature is the role of the QLNs interactions with the metal ions of the LDH layers. QLNs are able to establish coordination bonds with metal ions such as Mg^{2+}, Zn^{2+} or Al^{3+} with their 3-carboxyl and 4-oxo groups.[25] This interaction is dependent on the drug, the metal ions, and conditions such as pH.[26] HNal, for example, present complexation reactions with Mg^{2+} and Al^{3+} ions, which produce important changes in its properties, namely lipophilicity, solubility, acidity constant as well as in its bioavailability, permeation capacity and bactericidal action.[27–29] Consequently, these interactions are not only important to successfully obtain effective LDH-based DSs but also provide a tool for their customization.

In this work, we explored the properties of QLNs-loaded DSs based on Mg–Al LDHs, using basic form of HNal (Nal) as a probe, with emphasis on the synthesis of NPs and the interactions of Nal with Mg^{2+} ions. Nal-loaded DSs (LDH-Nal-DSs) were prepared by different coprecipitation methods and the composition, structure and morphology of the obtained samples were determined. Finally, the drug release profiles and the antimicrobial activity of the DSs were compared to that of the free drug.

2. Materials and methods

2.1. Materials

$MgCl_2{\cdot}6H_2O$ and $AlCl_3{\cdot}6H_2O$ (PA grade, Anedra®), nalidixic acid (HNal, Sigma Aldrich®), NaOH granules and 37% w w^{-1} HCl solution (PA grade, Cicarelli®), KH_2PO_4 and K_2HPO_4 (PA grade, Anedra®) and NaCl (PA grade, Parafarm®) were used without further treatment in the experiments. All solutions were prepared with purified water (18 MΩ MilliQ, Millipore System) and all experiments, unless otherwise stated, were performed at room temperature. The LDH syntheses were done using decarbonated water by boiling and N_2 bubbling. NaCl 0.9% w v^{-1} solution (NaCl0.9%) and phosphate buffer solutions at pH 5.8 (PBS5.8) and 7.4 (PBS7.4) were prepared according to USP specifications.

2.2. Synthesis of the LDH-Nal-DSs

2.2.1. Coprecipitation at variable pH. A 100 mL solution containing $MgCl_2$ (0.3 mol L^{-1}) and $AlCl_3$ (0.1 mol L^{-1}) was quickly added to a 200 mL solution containing NaOH (0.45 mol L^{-1}) and HNal (0.05 mol L^{-1}) under vigorous stirring provided by an Ultraturrax T18 BASIC agitator at 25 000 rpm. Once the addition was finished, the prepared solid was separated by centrifugation and washed twice with water. Subsequently, a suspension of the DS obtained (LDH-Nal-pHvar) in 400 mL of water was prepared and aged by hydrothermal treatment at 80 °C for 4 hours. A portion of this dispersion was freeze-dried to perform the chemical and structural characterization of the sample.

2.2.2. Coprecipitation at constant pH. A 100 mL solution containing $MgCl_2$ (0.3 mol L^{-1}) and $AlCl_3$ (0.1 mol L^{-1}) was added dropwise to a 200 mL solution containing 0.01 mol HNal, whose pH was previously set to 9. The pH of the media was maintained constant to this value by addition of 1 mol L^{-1} NaOH solution. Once the addition was finished, the DS obtained (LDH-Nal-pHcte) was processed according to that described in Section 2.2.1.

2.2.3. Reference samples. A sodium salt of the anionic form of nalixidic acid (NaNal) was prepared by neutralization of HNal with NaOH 1 mol L^{-1}, (final pH = 11), followed by lyophilization of the obtained solution. Also, a magnesium complex with the anionic form of nalixidic acid ($Mg(Nal)_2$) was obtained by mixing equivalent volumes of a 0.1 mol L^{-1} $MgCl_2$ solution and a 0.2 mol L^{-1} NaNal solution. The obtained solid was washed and lyophilized to perform its chemical and structural characterization. Finally, a chloride intercalated LDH (LDH-Cl) was prepared by the procedure described in Section 2.2.2. in absence of Nal anions.

2.3. Structural and morphological characterization

Mg/Al ratio was determined by energy dispersive X-ray spectroscopy (EDS) on pellets obtained by compression of 0.2 g of the corresponding sample at 2 tons in a 11 mm die. C and N content was determined by Pregl-Dumas method in a CHN 2400 Series II Elemental Analyzer, using cysteine as reference. Exchangeable Nal content was determined in 0.3 g L^{-1} dispersions in PBS7.4, equilibrated for 24 hours. After centrifugation, Nal concentration in the supernatants was determined by UV-Vis spectrometry (Shimadzu UV1601, Japan), at λ = 330 nm. Thermogravimetric and differential thermal analyses (TG/DTA) were performed in a Shimadzu DTG 60 instrument, under flowing air at a 10 °C min^{-1} slope. Powder X-ray diffraction (PXRD) patterns were recorded in a Phillips X'pert Pro instrument equipped with a Pixcell 1D detector using a Cu Kα lamp (λ = 1.5418 Å) at 40 kV and 40 mA in continuous mode. Fourier Transform Infrared Spectroscopy (FT-IR) spectra were measured in a Bruker IFS28 instrument using KBr pellets (1 : 100 sample : KBr ratio).

The hydrodynamic apparent diameter (d) and zeta potential (ζ) of the samples were determined by dynamic light scattering and electrophoretic light scattering measurements, respectively, using a Delsa Nano C instrument (Beckman Coulter). The size distributions were obtained by the CONTIN algorithm, while electrophoretic mobilities were converted to ζ using the Smoluchowski equation. Morphological images of the solids and EDS determinations were obtained in a Field Emission-Scanning Electron Microscopy (FE-SEM) Σigma instrument. To obtain SEM images, a drop of a 0.1 g L^{-1} dispersion of each sample was placed on a silicon wafer, dried at 60 °C and covered with a Cr layer.

2.4. Drug release studies

Drug release profiles were determined in a bicompartmental diffusion device (Franz cells) mounted with a semisynthetic cellulose membrane (12 kDa, Sigma-Aldrich®, USA). 1 mL of the DSs

(or the free drug, used as reference) dispersions was carefully placed in the donor compartment. It was kept in contact with 16.0 ± 0.7 mL of receptor medium (water, NaCl0.9%, PBS5.8 and PBS7.4) at 37 °C. 1.0 mL portions of receptor medium were withdrawn at different time intervals and replaced with equivalent volumes of preheated fresh medium. Drug concentration in the samples was determined by UV-Vis spectrometry, using calibration curves constructed for each receptor medium. All experiments were carried out in triplicate.

The mean release profiles were fitted according to following equations:[30,31]

$$\text{Zero-order model: } M_t = M_0 + k_0 \times t \quad (1)$$

$$\text{Higuchi model: } \frac{M_t}{M_0} = k_H \times t^{0.5} \quad (2)$$

$$\text{Peppas model: } \frac{M_t}{M_0} = k_P \times t^n \quad (3)$$

where M_0 is the initial amount of drug in the donor compartment, M_t is the amount of drug permeated at time t, and k_0, k_H and k_P are the corresponding kinetic constants. Finally, n parameter in the Peppas model equation (eqn (3)) characterizes the release mechanism. For n = 0.5 and n = 1, the equation is identical to that of zero order (eqn (1)) and Higuchi (eqn (2)) models, respectively, while n values between 0.5 and 1 indicate an anomalous process or superposition of both phenomena. When the drug release was stabilized within the time of the experiments, the data used for the fittings where those under 80% of the maximum cumulative drug release.

2.5. Antimicrobial studies

The antimicrobial activity of the LDH-Nal-DSs was evaluated against *Staphylococcus aureus* ATCC 25923 due to its incidence in topical infections.[5] The bacterial cultures were grown overnight at 37 °C in nutrient Mueller–Hinton medium and then diluted to 10^8 CFU mL^{-1}.

MIC assays were performed by the broth dilution method, where LDH-Nal-pHcte, LDH-Nal-pHvar and the pure drug were tested at different concentrations, corresponding to [Nal] = 8, 16, 32, 64, 128, 256 and 512 μg mL^{-1} in Mueller–Hinton broth medium placed in individual tubes. In order to do that, 1 mL of Mueller–Hinton broth (10^5 CFU mL^{-1}) was added to 1 mL of aliquot of each consecutive dilution. The microbial cultures were incubated at 37 °C for 24 hours and the MIC was determined by UV absorption measurements at λ = 600 nm of the obtained dispersions. Also, lawn cultures on Mueller Hinton agar plates were made with dispersions that contained a [Nal] above the MIC. These plates were inverted and incubated for 24 hours at 37 °C and finally, the number of colony forming units was counted. These experiments were performed in duplicate on separate.

Finally, the inhibition zone assay was used to compare the antimicrobial activity of LDH-Nal-DSs and the pure drug against *S. aureus*. The bacterial cultures (10^8 CFU mL^{-1}) were distributed over the surface of the Mueller–Hinton agar to obtain a uniform growth. In each plate, 4 stainless steel cylinders of the same size were placed on the surface of Mueller–Hinton agar and were filled with 100 μL of the corresponding sample dispersion ([Nal] = 512 μg mL^{-1}). The plates were incubated for 24 hours at 37 °C. Then, the diameters (mm) of the growth inhibition zone were carefully measured with a caliper.

3. Results and discussion

3.1. Synthesis and characterization of LDH-Nal-DSs

The structure of the LDH-Nal-DSs were studied by PXRD patterns (Fig. 1) and FT-IR spectra (Fig. 2). The PXRD patterns of both LDH-Nal-pHvar and LDH-Nal-pHcte (Fig. 1e and f, respectively) exhibited peaks corresponding to a LDH phase with a basal spacing of 8.1 Å. This basal spacing was similar to that of LDH-Cl (Fig. 1d), and it is typical of chloride intercalated LDHs.[32] Nevertheless, the chemical analysis of the samples (Table 1) indicated an important amount of Nal anions were incorporated to the solids. These results indicated that Nal was intercalated between LDH layers, which produced a strong structural disorder[33] and/or low layer stacking[34] that completely hindered diffraction on (0 0 l) plane for the Nal intercalated phase and also widened the 00l peaks corresponding to the chloride intercalated one. The Nal anions were also placed at the particle surface, where a portion of the positive charge generated by Al^{3+} ions are

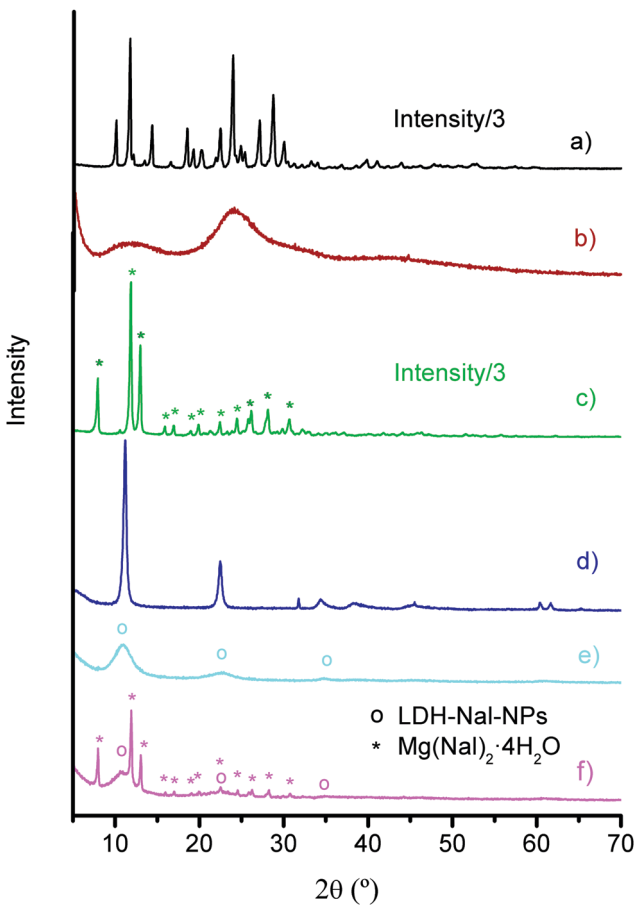

Fig. 1 PXRD patterns of (a) HNal, (b) NaNal, (c) $Mg(Nal)_2$, (d) LDH-Cl, (e) LDH-Nal-pHvar, (f) LDH-Nal-pHcte.

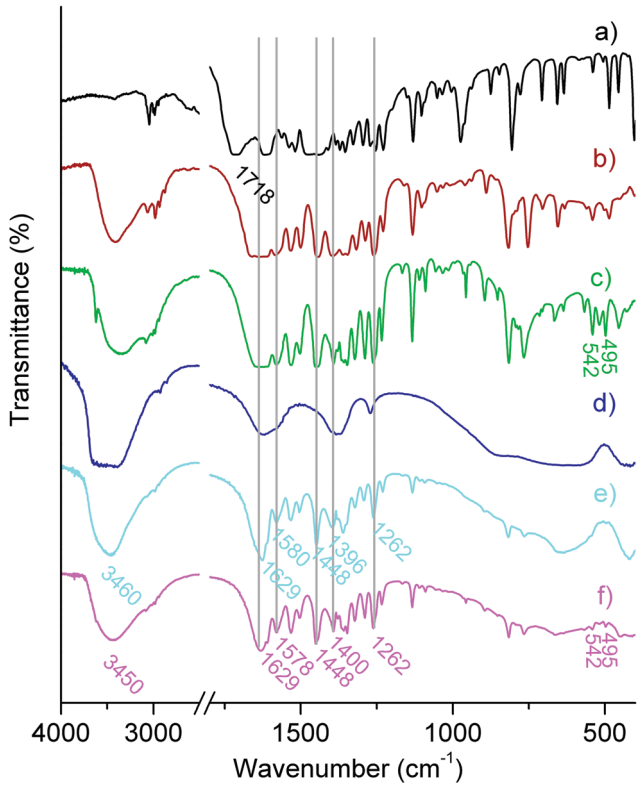

Fig. 2 FT-IR spectra of (a) HNal, (b) NaNal, (c) $Mg(Nal)_2$, (d) LDH-Cl, (e) LDH-Nal-pHvar, (f) LDH-Nal-pHcte. The main bands of Nal anions are indicated by grey lines.

located. This portion was particularly important for small LDH-NPs such as those observed by SEM (see below, Fig. 4). Instead, LDH-Nal-pHcte showed additional peaks, narrow and with high intensity, identical to those obtained in the pattern of the reference sample $Mg(Nal)_2$ (Fig. 1c). No peaks of HNal (Fig. 1a and Joint Committee on Powder Diffraction Standards PDF data number 30-1820) or NaNal (Fig. 1b) were observed in the patterns of the neither of the LDH-Nal-DSs, which indicates that neither form of the pure drug was present in the samples.

The incorporation of Nal anions and the presence of $Mg(Nal)_2$ in LDH-Nal-pHcte were confirmed by FT-IR spectra (Fig. 2). Both LDH-Nal-DSs (Fig. 2e and f) exhibited bands of Nal anions at 1570–1590 cm^{-1} and 1390–1400 cm^{-1} ranges ($\nu_{asym,COO}$ and $\nu_{sym,COO}$), 1629 cm^{-1} (ν_{CO}, ketone group), 1448 cm^{-1} (δ_{C-H}) and 1262 cm^{-1} (ν_{CO} + ν_{NO} coupling). The positions of these bands were similar between both samples and also with those of NaNal and $Mg(Nal)_2$ reference samples (Fig. 2b and c). On the contrary, bands at 1718 cm^{-1} (ν_{COOH}) were absent, which confirmed that HNal (Fig. 2a) was not present in the LDH-Nal-DSs. Also, their spectra showed wide bands corresponding to hydroxyl anions as well as wide bands in the 900–400 cm^{-1} range due to ν_{M-O} and ν_{M-O-M} of LDH layers,[35] analogous to those of LDH-Cl (Fig. 2d). Finally, LDH-Nal-pHcte presented bands at 542 and 495 cm^{-1}, similar to those obtained for $Mg(Nal)_2$ and to those obtained Nal complexes with Ca^{2+} or Fe^{3+}.[36] On the contrary, these bands were absent in LDH-Nal-pHvar spectrum.

The LDH-Nal-DSs composition was explained by two competing reactions, namely the formation of a Nal-containing LDH and the precipitation of $Mg(Nal)_2$, a coordination compound with a 1 : 2 Mg : Nal ratio.[28] Titration curves of the Mg^{2+} and Al^{3+} solutions in the presence of HNal (Fig. S1, ESI†) indicated that $Mg(Nal)_2$ was formed upon nalixidate dissolution in the presence of Mg^{2+} ions. Nevertheless, increasing the pH of the media produced the dissolution of the complex and the precipitation of Mg^{2+} ions as part of LDH layers. This reaction can be written as:

$$Al(OH)_{3(s)} + 2.5Mg^{2+}_{(aq)} + 5OH^{-}_{(aq)} + 0.5Mg(Nal)_2{\cdot}4H_2O_{(s)} \rightarrow Mg_3Al(OH)_8Nal{\cdot}nH_2O_{(s)} \quad (4)$$

Thus, the synthesis of LDH-Nal-pHvar involved the addition of the metal salts solution to a solution with a large [OH^-] and [Nal][37] and, consequently, the formation of the Nal containing LDH phase was favored. On the other hand, the synthesis method of LDH-Nal-pHcte maintained a low [OH^-] (pH = 9) during the whole process[38] in a medium with a high [Nal] and, consequently the formation of $Mg(Nal)_2$ was more favorable than for LDH-Nal-pHvar. $Mg(Nal)_2$ was also formed by Nal interaction with LDHs, as demonstrated by adsorption experiments on LDH-Cl (Fig. S2, ESI†). In these experiments, Nal anions showed a low affinity for LDH layers and they were incorporated by two main processes: adsorption at low [Nal] and $Mg(Nal)_2$ precipitation at high ones. Due to the large particle size and stacking of LDH-Cl sample, Nal incorporation at the surface of LDH-Cl particles was quite lower than for the samples obtained by direct synthesis by coprecipitation. A complete description of both titration and adsorption experiments are included with the Fig. S1 and S2 of the ESI.†

The incorporation of Nal anions to the LDH phase was confirmed by the TG/DTA curves (Fig. 3). Thus, LDH-Nal-pHvar (Fig. 3e)

Table 1 Chemical analyses and proposed formulae of the LDH-Nal-DSs. Theoretical values according to the proposed formulae are given between parentheses

Sample	Mg : Al[a]	% C[b]	%N[b]	$\%H_2O$[c]	$\%w_{750}$[d]	$\%Nal_{exc}$[e]	Formula
LDH-Cl	2.8 (2.8)	—	—	14.1 (14.0)	55.9 (54.2)	—	$Mg_{0.74}Al_{0.26}(OH)_2Cl_{0.26}{\cdot}0.62H_2O$
LDH-Nal-pHvar	3.3 (3.3)	18.3 (18.0)	3.3 (3.4)	15.3 (15.3)	39.0 (41.2)	32.0 (27.9)	$Mg_{0.77}Al_{0.23}(OH)_2Nal_{0.13}Cl_{0.10}{\cdot}0.88H_2O$
LDH-Nal-pHcte	2.4 (2.4)	28.4 (26.7)	5.1 (5.1)	(14.0) (14.1)	29.5 (31.9)	35.7 (36.1)	$Mg_{0.70}Al_{0.30}(OH)_{2.00}Nal_{0.22}Cl_{0.08}{\cdot}0.99H_2O + 0.02Mg(Nal)_2{\cdot}4H_2O$
$Mg(Nal)_2$	—	50.4 (51.6)	10.2 (10.0)	12.7 (12.9)	6.3 (7.2)	5.4 (0)	$Mg(Nal)_2{\cdot}4H_2O$

[a] mol mol^{-1}, determined by EDS. [b] w w^{-1}, as determined by the Pregl–Dumas method. [c] Residual weight at 175 °C as determined by TG analysis (Fig. 3). [d] Residual weight at 750 °C as determined by TG analysis (Fig. 3), theoretical values were calculated considering that the only residues at this temperature are metal oxides. [e] Exchangeable Nal percentage (w w^{-1}), determined by UV-Vis spectrometry in 1 g L^{-1} dispersions in PBS7.4.

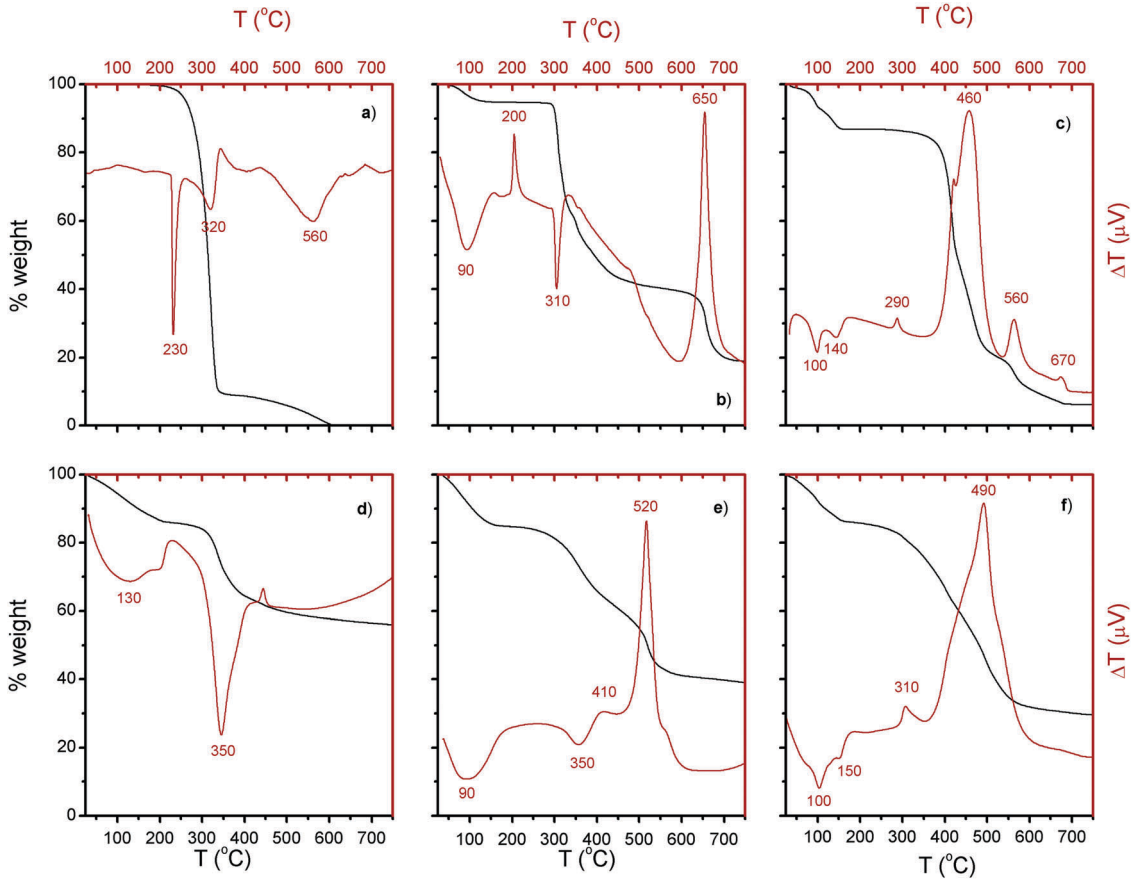

Fig. 3 TG/DTA curves of (a) HNal, (b) NaNal, (c) $Mg(Nal)_2$, (d) LDH-Cl, (e) LDH-Nal-pHvar, (f) LDH-Nal-pHcte.

showed the three main processes involved in LDHs thermal decomposition, namely dehydration, dehydroxylation and anion decomposition. Dehydration process extended up to 180 °C approximately with the peak of the associated endothermic effect centered at 90 °C, while the weight loss due to dehydroxylation and loss of the Nal anion was produced between 250 °C and 600 °C, where the main peak was exothermic and registered at 520 °C. The peaks obtained for this sample was quite different to those obtained for either HNal or NaNal (Fig. 3a and b, respectively), which confirmed that neither of the pure drug forms was precipitated together with the LDH phase. Alternatively, LDH-Nal-pHcte (Fig. 3f) curve showed an intermediate behavior between those of LDH-Nal-pHvar and $Mg(Nal)_2$ (Fig. 3c). The curve of the latter presented two endothermic effects, centered at 100 and 140 °C, assigned to dehydration, while the drug oxidation produced a sudden weight loss that started at 400 °C and presented exothermic peaks at 460, 560 and 670 °C. The $\%w_{750}$ value for $Mg(Nal)_2$ (6.3%) was concordant with the chemical formula $Mg(Nal)_2{\cdot}4H_2O$, considering MgO as the only residue at this temperature. Finally, LDH-Nal-pHcte showed an intermediate behavior between LDH-Nal-pHvar and $Mg(Nal)_2$. Thus, the dehydration step (up to 200 °C) produced a couple of thermal events similar to those registered for $Mg(Nal)_2$, but they were framed inside a wide band similar to that of LDH-Nal-pHvar. Also, the continuous weight loss in the 250–500 °C range and the exothermic peak at 490 °C were similar to those of LDH-Nal-pHvar. Nevertheless, the presence of the complex $Mg(Nal)_2{\cdot}4H_2O$ in the sample LDH-Nal-pHcte produced a widening of the exothermic peak and its displacement to a temperature intermediate between those of LDH-Nal-pHvar and $Mg(Nal)_2$. The weight of the residue at 750 °C ($\%w_{750}$) was 29.5% for this sample, which was lower than that of LDH-Nal-pHvar (39.0%) but much higher than that obtained for $Mg(Nal)_2$ reference sample.

The structural characterization, together with the weight losses obtained in the TG curves and the elemental analysis performed to the samples, allowed establishing the chemical formulae of the LDH-Nal-DSs (Table 1). There was a good correlation between the experimental values and those calculated on the basis of the proposed formula, which indicated that they were a good approximation to the actual composition of the LDH-Nal-DSs. LDH-Nal-pHvar formula was proposed considering the presence of only one LDH phase containing both Nal^- and Cl^- anions. The Mg : Al ratio (3.3 : 1) was similar to that of the starting solution, while the Nal content corresponded to 54% of the anion exchange capacity (AEC) of the LDH layers. On the other hand, LDH-Nal-pHcte formula considered the presence of two phases, one corresponding to a Nal intercalated LDH with a 2.3 : 1 Mg : Al ratio and a Nal content equivalent to 70% of the AEC and another corresponding to the $Mg(Nal)_2$ salt ($Mg(Nal)_2{\cdot}4H_2O$). According to the chemical

formula proposed, approximately 85% of the NaI anions were included between the LDH layers, while only 15% were in the $Mg(NaI)_2$ salt. The percentage of exchangeable NaI ($\%NaI_{exc}$), determined by the drug release produced in PBS7.4, exhibited a good fitting for both LDH-NaI-pHvar and LDH-NaI-pHcte. Nevertheless, for the latter, it was considered that NaI ions in $Mg(NaI)_2{\cdot}4H_2O$ were not released in this medium, in good accord with the $\%NaI_{exc}$ (<6%) of this reference sample.

LDH-NaI-pHvar presented a wide size distribution (Fig. 4A) with a maximum at 342 nm which was in the same order to that obtained for LDH-Cl (76 nm). Nevertheless, while the SEM images of LDH-Cl-NPs (Fig. 4B) showed thick, regularly shaped particles with sizes within the size range similar to those obtained by DLS (between 50 and 200 nm according to Fig. 4A), the LDH-NaI-NPs in Fig. 4D presented particle size between 30 and 40 nm, quite below to the size distribution obtained by DLS (between 100 nm and 1 μm), which was associated to aggregation processes. The morphology of LDH-NaI-pHvar (Fig. 4D) particles (thin, small, and irregularly shaped) was consistent with the low crystallinity and layer stacking indicated by its PXRD patterns. On the other hand, the particle size distribution of LDH-NaI-pHcte was displaced to the micrometric range, with a wide size distribution. The particle size increase for LDH-NaI-pHcte was not due to aggregation of LDH-NPs but to the presence of the $Mg(NaI)_2$ phase. Effectively, the SEM images of LDH-NaI-pHcte (Fig. 4E and F) showed the same small particles observed for LDH-NaI-pHvar and assigned to the LDH-NaI-NPs phase, but also needle-shaped particles with a length of a few μm assigned to the $Mg(NaI)_2$ complex. These particles present a similar shape to those of $Mg(NaI)_2$ sample (Fig. 4C) but, in the case of LDH-NaI-pHcte, they were quite larger and they were covered by LDH-NaI-NPs. These results confirmed the presence of a mixture of LDH-NaI-NPs and $Mg(NaI)_2$ particles. Although the particles of the former were more numerous than those of the latter in Fig. 4E and F, the size distribution by DLS (Fig. 4A) overweighed the presence of large particles due to the larger light dispersion capacity of large particles.[39]

3.2. Drug release studies

NaI release from LDH-NaI-DSs was studied to evaluate their performance for topical administration (Fig. 5) and the results obtained were compared to those of the free drug. Fitting of release data with representative kinetic models (zero order, Higuchi and Peppas) allowed to parameterize the kinetic behavior and to give a insight on the drug release mechanism (Table 2). Theoretical kinetic profiles obtained with the better fits of each sample and medium (marked with * in Table 2) were included in Fig. 5 to provide a guide for the eye and an indication of the goodness-of-fit of these models.

The free drug showed similar behaviors towards water, NaCl0.9% and PBS5.8, which produced cumulative NaI releases at the end of the experiment ($\%NaI_{360}$) around 13%. Also, the release profiles were linear in all cases, as indicated by the regression coefficient values (R^2), above 0.99 for zero order model. Then, the determining step for NaI release from the free drug was dissolution from the particle surface, which was limited for all these media due to the low solubility of HNaI. Instead, $\%NaI_{360}$ reached around 33% for PBS7.4 and, contrarily to that obtained in the previous media, drug release stabilized within the time of the experiment. Nevertheless, the best fit for the profile (up to 80% of the overall release at the plateau) was obtained for Peppas model with $n \sim 1$, which, as previously stated, relates to a zero-order model. Consequently, drug dissolution was still the rate determining step in this media, and the only difference was a HNaI solubility enhancement due to neutral pH of the receptor media.

On the other hand, the release profiles from LDH-NaI-pHvar were quite dependent on the receptor media. Thus, $\%NaI_{360}$ increased in the order water ≪ PBS5.8 < NaCl0.9% ≪ PBS7.4 (6, 12, 14 and 22%, respectively). The best fits were obtained for Higuchi model, which indicated that diffusion was the determining

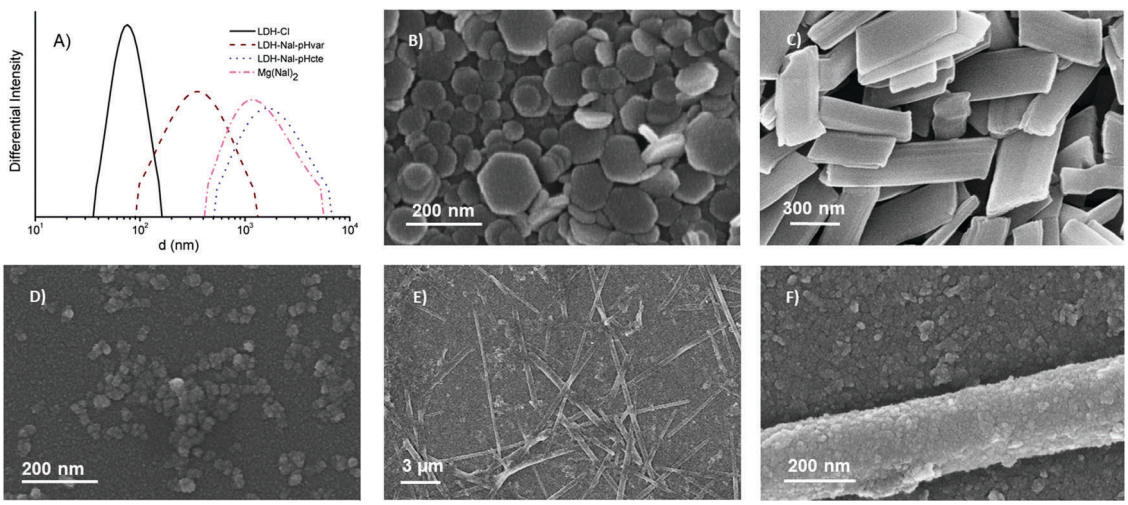

Fig. 4 Intensity size distribution of LDH-NaI-DSs and reference samples (A). SEM images of LDH-Cl (B), $Mg(NaI)_2$ (C), LDH-NaI-pHvar (D), LDH-NaI-pHcte (E and F).

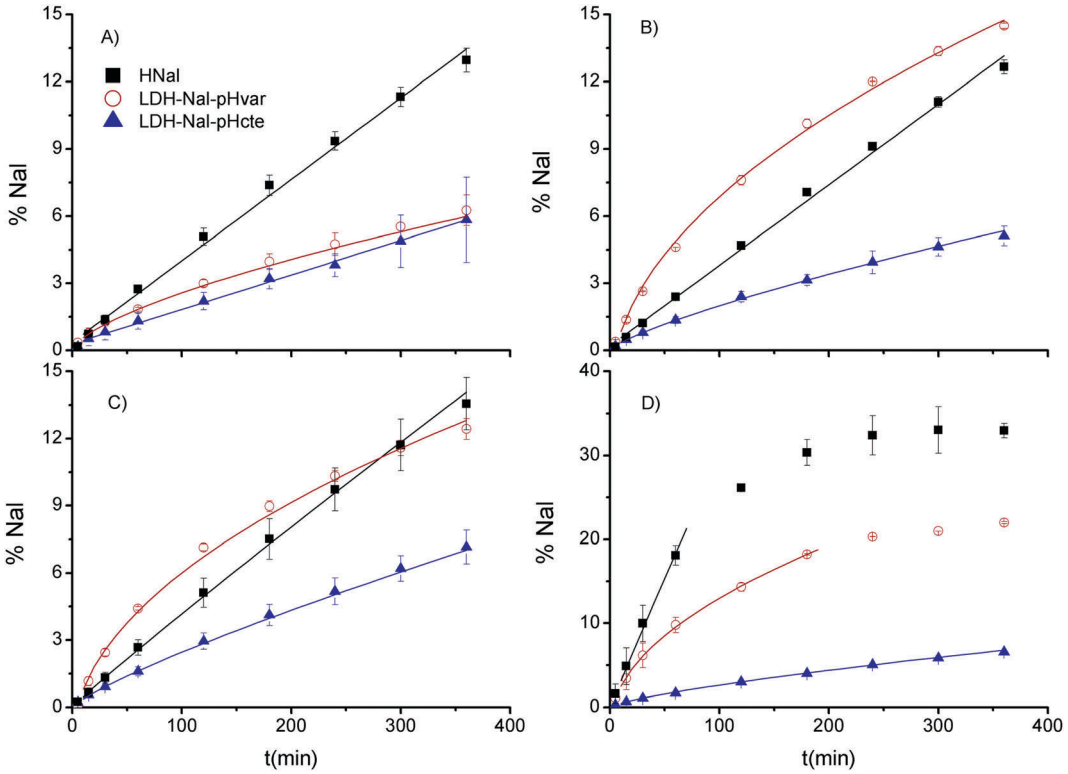

Fig. 5 *In vitro* Nal release profile from the free drug, LDH-Nal-pHvar and LDH-Nal-pHcte, placed as dispersions in the donor compartment and released toward (A) water, (B) NaCl0.9%, (C) PBS5.8 and (D) PBS7.4. Lines are calculated release profiles using the best fitting model for each experiment, marked with asterisks (*) in Table 2.

Table 2 Kinetic data obtained by modeling Nal release profiles with zero order, Higuchi and Peppas model. Fittings with the best R^2 are marked with asterisks

Kinetic model		Zero order			Higuchi			Peppas		
Release media	Sample	$\%Nal_0$	K_Z	R^2	$\%Nal_0$	K_H	R^2	$-\log(K_P)$	n	R^2
Water	HNal	0.36*	0.0364*	0.995*	−2.6	0.78	0.981	1.37	0.99	0.993
	LDH-Nal-pHvar	0.71	0.0163	0.984	−0.66	0.35	0.994	0.90*	0.66*	0.999*
	LDH-Nal-pHcte	0.29*	0.0154*	0.997*	−0.95	0.33	0.971	1.31	0.80	0.995
NaCl 0.9%	HNal	0.20*	0.036*	0.997*	−2.71	0.77	0.975	1.46	1.02	0.997
	LDH-Nal-pHvar	1.57	0.040	0.960	−1.94*	0.88*	0.998*	0.88	0.83	0.985
	LDH-Nal-pHcte	0.41	0.014	0.985	−0.76	0.30	0.992	1.24*	0.77*	0.999*
PBS pH = 5.8	HNal	0.29	0.038	0.997	−2.79	0.81	0.976	1.28*	0.95*	1.000*
	LDH-Nal-pHvar	1.50	0.034	0.939	−1.6*	0.76*	0.997*	1.67	1.17	0.861
	LDH-Nal-pHcte	0.36	0.020	0.995	−1.25	0.42	0.982	1.25*	0.82*	1.000*
PBS pH = 7.4	HNal	0.42	0.30	0.997	−6.02	3.03	0.986	0.48*	0.98*	0.999*
	LDH-Nal-pHvar	2.45	0.094	0.959	−2.31*	1.53*	1.000*	0.42	0.77	0.980
	LDH-Nal-pHcte	0.54	0.018	0.988	−0.95	0.38	0.990	1.06*	0.74*	1.000*

step of the drug release. Such behavior is typical of LDHs at pHs above 5, where layers dissolution is minimized and anion exchange is the main release mechanism.[40,41] The exception was the release profile for water, whose best fit was obtained for Peppas model with $n = 0.66$. Anion exchange was limited in this media by the absence of anions, and other processes, such as matrix dissolution, became relevant. Oppositely, the fastest release was observed for PBS7.4 due to presence of divalent HPO_4^{2-} anions, which present high affinity for LDHs.[13]

Finally, the presence of $Mg(Nal)_2$ in LDH-Nal-pHcte produced relevant changes respect to that obtained for LDH-Nal-pHvar. $\%Nal_{360}$ was lower (around 6–7%) for the former and quite independent of the receptor media. Also, the best fits were not obtained for Higuchi model, which indicated a change in the release mechanism. In the case of water, the best fit was obtained for the zero-order model, which indicated that anion exchange was completely suppressed. For the remaining media, the best fits were obtained for Peppas model with n values

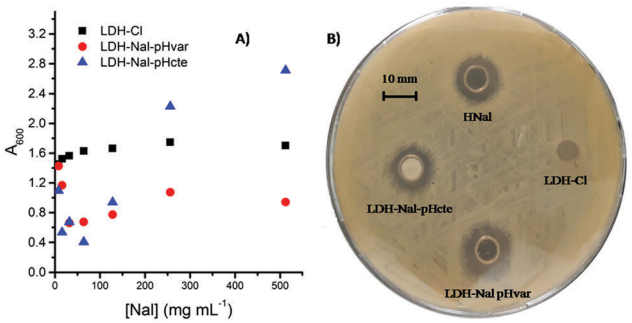

Fig. 6 Microbiological studies of LDH-Nal-DSs and the pure drug. (A) Absorbance at λ = 600 nm of cultures (A_{600}) *vs.* [Nal], after 24 hours incubation, (B) zones of bacterial inhibition at [Nal] = 512 μg mL^{-1} in Mueller Hinton agar plates seeded with 10^8 CFU bacterial cultures.

between 0.74 and 0.82. These results indicated that $Mg(Nal)_2$ dissolution was an important drug release mechanism for LDH-Nal-pHcte. Due to the protonation reactions of Nal anions (Fig. S1, ESI†), $Mg(Nal)_2$ increased its solubility at pHs lower than 8. This mechanism explained that, contrarily to LDH-Nal-pHvar, the $\%Nal_{360}$ values were less affected by the anions present in the release medium. Nevertheless, there was an increasing contribution of the anion exchange mechanism with the affinity of the anions in the release media, as demonstrated by the decreasing n values for water (no exchanging anions), 0.9% NaCl (Cl^-), PBS5.8 (mainly $H_2PO_4^-$ anions) and PBS7.4 (mainly HPO_4^{2-} anions).

These results indicated that, although both LDH-Nal-DSs presented good properties for their application in topical formulations, their characteristics were quite different. Thus, Nal release from LDH-Nal-pHvar toward both PBS5.8 and PBS7.4, which simulate intact and damage skin, respectively, indicated a pH-sensitive behavior that was not present on LDH-Nal-pHcte. This behavior would lead to a faster release in an injured area, where it is more needed. Also, due the faster drug release from LDH-Nal-pHvar than from LDH-Nal-pHcte, the former was expected to achieve more rapidly MIC values, and the latter to provide a more sustained action independently of the release medium.

3.3. Antimicrobial activity

The microbiological studies (Fig. 6) showed that LDH-Nal-DSs possessed better activity than the pure drug. Thus, the MIC determined for the pure drug was 128 μg mL^{-1}, while it was 64 and 32 μg mL^{-1} for LDH-Nal-pHcte and LDH-Nal-pHvar, respectively (Fig. 6A). The larger activity of LDH-Nal-DSs was related exclusively to an enhancement of the antimicrobial action of Nal, as demonstrated by the absence of antimicrobial activity for LDH-Cl in the concentration range studied. The MIC diminution was explained by the mechanism of action of HNal and effects produced by its vehiculization as LDH-Nal-NPs. The antimicrobial activity of Nal is based on the interference with the synthesis of nucleic acids[42] and, consequently, permeation of the bacterial cell membrane is essential to its antimicrobial action. Due to the positive charge and size of the LDH-Nal-NPs, they are able to interact with the cell membrane, increasing in Nal permeability.[24,43]

The dispersions of the LDH-Nal-DSs became increasingly turbid at large [Nal], which was not due only to an increasing particle concentration, but also to an increasing bacterial proliferation, as determined by the colony forming units count (Fig. S3, ESI†). Nevertheless, this is not an uncommon behavior for QLNs:[44] *i.e.*, Nal presents its higher activity in the 50–200 μg mL^{-1} concentration range for most Gram-negative bacteria, while its activity decrease at large concentrations.[45] This effect was enhanced for LDH-Nal-NPs due to the permeation enhancement proposed above.

These results were complemented with inhibition zone assays (Fig. 6B). The diameter of the inhibitory zone for pure Nal was 12 mm, which indicated its poor antimicrobial activity against *S. aureus*. LDH-Nal-pHvar presented a slightly larger protection area (14 mm) than the pure drug, which was in good agreement with the lower MIC obtained for this sample. Also, the diameter of the inhibitory zone for LDH-Nal-pHcte was the same of the pure drug (12 mm), which was consistent with its higher MIC and its slower release kinetics compared to LDH-Nal-pHvar.

4. Conclusions

Layered double hydroxide-based delivery systems containing the basic form of nalidixic acid (LDH-Nal-DSs) were prepared using different synthesis procedures. Pure Nal-containing LDH nanoparticles (LDH-Nal-NPs) were obtained by coprecipitation at variable pH, while an additional phase, corresponding to a $Mg(Nal)_2{\cdot}4H_2O$ complex, was obtained for the one at constant pH (LDH-Nal-pHcte). Drug release from LDH-Nal-NPs was produced mainly by an anion exchange mechanism and its rate was dependent on the exchanging anions concentration. The presence of $Mg(Nal)_2$ in LDH-Nal-pHcte led to a release rate diminution, which was explained by the change in the main release mechanism due to the influence of $Mg(Nal)_2$ dissolution in this sample. LDH-Nal-NPs also produced an enhanced antimicrobial activity, which was related to their positive ζ and the consequent interactions with the bacterial cell membrane, negatively charged. These results indicate that LDH-NPs portray interesting features as DSs for (fluoro)quinolones, but careful control of the synthesis method is necessary to control the interactions of these drugs with the metal ions of LDHs and, therefore, the properties of the resulting DSs.

Conflicts of interest

There are no conflicts to declare.

Acknowledgements

Salguero Y thanks to Secretaría de Educación Superior, Ciencia, Tecnología e Innovación (SENESCYT) de la República del Ecuador for her master fellowship. García MC thanks to CONICET for her postdoctoral fellowship. Economic supports by SeCyT-UNC, project number 05/C585, FONCyT, project PICT 12/0634, and

CONICET, PIP 11220120100575, are gratefully acknowledged. SEM images were obtained at LAMARX.

References

1 J. S. Wolfson and D. C. Hooper, *Antimicrob. Agents Chemother.*, 1985, **28**, 581–586.
2 M. H. Xiong, Y. Bao, X. Z. Yang, Y. H. Zhu and J. Wang, *Adv. Drug Delivery Rev.*, 2014, **78**, 63–76.
3 P. Gao, X. Nie, M. Zou, Y. Shi and G. Cheng, *J. Antibiot.*, 2011, **64**, 625–634.
4 R. S. Kalhapure, N. Suleman, C. Mocktar, N. Seedat and T. Govender, *J. Pharm. Sci.*, 2015, **104**, 872–905.
5 M. C. García, J. C. Cuggino, C. I. Rosset, P. L. Páez, M. C. Strumia, R. H. Manzo, F. L. Alovero, C. I. Alvarez Igarzabal and A. F. Jimenez-Kairuz, *Mater. Sci. Eng., C*, 2016, **69**, 236–246.
6 V. Rives, M. del Arco and C. Martín, *Appl. Clay Sci.*, 2014, **88–89**, 239–269.
7 M. Jafarbeglou, M. Abdouss, A. M. Shoushtari and M. Jafarbeglou, *RSC Adv.*, 2016, **6**, 50002–50016.
8 D. Mosangi, L. Moyo, S. Kesavan Pillai and S. S. Ray, *RSC Adv.*, 2016, **6**, 105862–105870.
9 Z.-L. Liu, D.-Y. Tian, S.-P. Li, X.-D. Li and T.-H. Lu, *Int. J. Pharm.*, 2014, **473**, 414–425.
10 M. A. Djebbi, A. Elabed, Z. Bouaziz, M. Sadiki, S. Elabed, P. Namour, N. Jaffrezic-Renault and A. B. H. Amara, *Int. J. Pharm.*, 2016, **515**, 422–430.
11 E. P. Komarala, S. Doshi, S. Thiyagarajan, M. Aslam and D. Bahadur, *New J. Chem.*, 2018, **42**, 129–136.
12 S. P. Newman and W. Jones, *New J. Chem.*, 1998, **22**, 105–115.
13 R. Rojas, M. C. Palena, A. F. Jimenez-Kairuz, R. H. Manzo and C. E. Giacomelli, *Appl. Clay Sci.*, 2012, **62–63**, 15–20.
14 Z. Gu, A. C. Thomas, Z. P. Xu, J. H. Campbell, G. Qing and M. Lu, *Chem. Mater.*, 2008, 3715–3722.
15 L. Perioli, V. Ambrogi, L. di Nauta, M. Nocchetti and C. Rossi, *Appl. Clay Sci.*, 2011, **51**, 407–413.
16 G. Choi, J.-H. Lee, Y.-J. Oh, Y. Bin Choy, M. C. Park, H. C. Chang and J.-H. Choy, *Int. J. Pharm.*, 2010, **402**, 117–122.
17 W. Zhang, P. Jiang, Y. Chen, P. Luo, G. Li, B. Zheng, W. Chen, Z. Mao and C. Gao, *Nanoscale*, 2016, **8**, 9572–9582.
18 D. Hesse, M. Badar, A. Bleich, A. Smoczek, S. Glage, M. Kieke, P. Behrens, P. P. Müller, K. H. Esser, M. Stieve and N. K. Prenzler, *J. Mater. Sci.: Mater. Med.*, 2013, **24**, 129–136.
19 Z. Rezvani, M. Shahbaei and M. S. Zolfaghar Rezvani, *Polym. Polym. Compos.*, 2008, **16**, 101–113.
20 F. Duda, M. Kieke, F. Waltz, M. E. Schweinefuss, M. Badar, P. P. Müller, K. H. Esser, T. Lenarz, P. Behrens and N. K. Prenzler, *J. Mater. Sci.: Mater. Med.*, 2015, **26**, 5334.
21 Y. Li, H.-Y. Bi, H. Li, X.-M. Mao and Y.-Q. Liang, *Mater. Sci. Eng., C*, 2017, **78**, 886–891.
22 H. Nabipour, M. H. Sadr and N. Thomas, *New J. Chem.*, 2016, **40**, 238–244.
23 B. Kutlu, P. Schröttner, A. Leuteritz, R. Boldt, E. Jacobs and G. Heinrich, *Mater. Sci. Eng., C*, 2014, **41**, 8–16.
24 S. Malekkhaiat Haffner, L. Nystrom, R. Nordstrom, Z. P. Xu, M. Davoudi, A. Schmidtchen and M. Malmsten, *Phys. Chem. Chem. Phys.*, 2017, **19**, 23832–23842.
25 I. Turel, *Coord. Chem. Rev.*, 2002, **232**, 27–47.
26 B. L. Lomaestro and G. R. Bailie, *Drugs*, 2001, **25**, 411–416.
27 M. Nakano, M. Yamamoto and T. Arita, *Chem. Pharm. Bull.*, 1978, **26**, 1505–1510.
28 N. B. Behrens, G. M. Diaz and D. M. L. Goodgame, *Inorg. Chim. Acta*, 1986, **125**, 21–26.
29 A. J. G. Bailey, A. Cole, J. Goodfield, P. M. May, M. E. Dreyfuss, J. M. Midgley and D. R. Williams, *Int. J. Pharm.*, 1984, **22**, 283–290.
30 P. Costa and J. M. Sousa Lobo, *Eur. J. Pharm. Sci.*, 2001, **13**, 123–133.
31 J. Siepmann and N. A. Peppas, *Adv. Drug Delivery Rev.*, 2001, **48**, 139–157.
32 V. A. Drits and A. S. Bookin, in *Layered Double hydroxides: Present and Future*, ed. V. Rives, Nova Science, New York, 2001, pp. 39–92.
33 D. Mosangi, S. Kesavan Pillai, L. Moyo and S. S. Ray, *RSC Adv.*, 2016, **6**, 77709–77716.
34 S. P. Lonkar, A. Leuteritz and G. Heinrich, *RSC Adv.*, 2013, **3**, 1495–1501.
35 J. T. Kloprogge and R. L. Frost, in *Layered Double Hydroxides: Present and Future*, ed. V. Rives, Nova Science Publishers, New York, 2001, pp. 139–192.
36 F. A. I. Al-Khodir and M. S. Refat, *J. Mol. Struct.*, 2015, **1094**, 22–35.
37 J. S. Valente, M. Sánchez-Cantú, E. Lima and F. Figueras, *Chem. Mater.*, 2009, **21**, 5809–5818.
38 E. M. Seftel, E. Popovici, M. Mertens, K. De Witte, G. Van Tendeloo, P. Cool and E. F. Vansant, *Microporous Mesoporous Mater.*, 2008, **113**, 296–304.
39 J. Stetefeld, S. A. McKenna and T. R. Patel, *Biophys. Rev.*, 2016, **8**, 409–427.
40 M. del Arco, A. Fernandez, C. Martin and V. Rives, *Appl. Clay Sci.*, 2009, **42**, 538–544.
41 M. L. Parello, R. Rojas and C. E. Giacomelli, *J. Colloid Interface Sci.*, 2010, **351**, 134–139.
42 F. C. Tenover, *Am. J. Infect. Control*, 2006, **34**, 3–9.
43 C. Vasti, V. Pfaffen, E. Ambroggio, M. R. Galiano, R. Rojas and C. E. Giacomelli, *Appl. Clay Sci.*, 2017, **137**, 151–159.
44 G. Cheng, H. Hao, M. Dai, Z. Liu and Z. Yuan, *Eur. J. Med. Chem.*, 2013, **66**, 555–562.
45 G. C. Crumplin and J. T. Smith, *Antimicrob. Agents Chemother.*, 1975, **8**, 251–261.

